J Mol Model (2008) 14:353–366
DOI 10.1007/s00894-008-0277-0

ORIGINAL PAPER

DFT-based molecular modeling and vibrational study of the La(III) complex of 3,3′-(benzylidene)bis(4-hydroxycoumarin)

Tzvetan Mihaylov · Natasha Trendafilova · Ivelina Georgieva

Received: 15 September 2007 / Accepted: 24 January 2008 / Published online: 20 February 2008

Abstract Molecular modeling of the La(III) complex of 3,3′-(benzylidene)bis(4-hydroxycoumarin) (PhDC) was performed using density functional theory (DFT) methods at B3LYP/6-31G(d) and BP86/TZP levels. Both Stuttgart-Dresden effective core potential and ZORA approximation were applied to the La(III) center. The electron density distribution and the nucleophilic centers of the deprotonated ligand $PhDC^{2-}$ in a solvent environment were estimated on the basis of Hirshfeld atomic charges, electrostatic potential values at the nuclei, and Nalewajski-Mrozek bond orders. In accordance with the empirical formula La(PhDC)(OH)(H_2O), a chain structure of the complex was simulated by means of two types of molecular fragment: (1) two La(III) cations bound to one $PhDC^{2-}$ ligand, and (2) two $PhDC^{2-}$ ligands bound to one La(III) cation. Different orientations of $PhDC^{2-}$, OH^- and H_2O ligands in the La(III) complexes were investigated using 20 possible $[La(PhDC^{2-})_2(OH)(H_2O)]^{2-}$ fragments. Energy calculations predicted that the prism-like structure based on "tail-head" *cis*-LML2 type binding and stabilized via HO...HOH intramolecular hydrogen bonds is the most probable structure for the La(III) complex. The calculated vibrational spectrum of the lowest energy La(III) model fragment is in very good agreement with the experimental IR spectrum of the complex, supporting the suggested ligand binding mode to La(III) in a chain structure, namely, every $PhDC^{2-}$ interacts with two La(III) cations through both carbonylic and both hydroxylic oxygens, and every La(III) cation binds four oxygen atoms of two different $PhDC^{2-}$.

T. Mihaylov · N. Trendafilova (✉) · I. Georgieva
Institute of General and Inorganic Chemistry,
Bulgarian Academy of Sciences,
1113 Sofia, Bulgaria
e-mail: ntrend@svr.igic.bas.bg

Keywords Molecular modeling · 3,3′-(Benzylidene)bis(4-hydroxycoumarin) · Lanthanum(III) complex · Density functional theory

Introduction

Coumarins are natural compounds with diverse biological activities [1–8]. Recently, coumarin derivatives have attracted increasing interest in the area of cancer drug development [9]. Along with pure organic compounds, many recent studies have reported rare earth metal complexes of coumarin derivatives with marked cytotoxic activities. It has been shown that lanthanide complexes of mendiaxon, warfarin, coumachlor and niffcoumar displayed antitumor activity against P3HR1, K-562, and THP-1 cell lines. The metal complexes mentioned above have stronger cell proliferation-inhibiting effects as compared to the inorganic salts [10–15].

Recently, new complexes of La(III), Ce(III), Nd(III) and Zr(IV) with phenyl and series of pyridyl substituted bis(4-hydroxycoumarin)s, i.e., 3,3′-(benzylidene)bis(4-hydroxycoumarin) (PhDC) (Fig. 1), 3,3′-(*o*-pyridinomethylene)bis(4-hydroxycoumarin), 3,3′-(*m*-pyridinomethylene) bis(4-hydroxycoumarin), and 3,3′-(*p*-pyridinomethylene)bis(4-hydroxycoumarin), have been synthesized and characterized [16–21]. The complexes have shown clear in vitro cytotoxic activity in micromolar concentrations. The La(III) complex of PhDC exhibits a significant cytotoxic effect on the acute myeloid leukemia derived HL-60 cells and the chronic myeloid leukemia (CML)-derived cell line BV-173 [22]. The cytotoxic activity of the Ce(III) complex of PhDC against K-565, LAMA-84, BV-173 and HL-60 cells has also been demonstrated [21]. To the best of our knowledge, no X-ray structural data on the Ln(III)

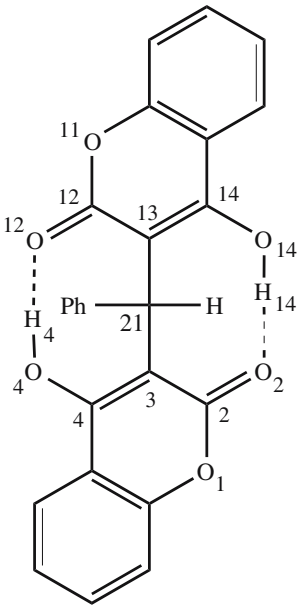

Fig. 1 Schematic presentation of 3,3′-(benzylidene)bis-(4-hydroxycoumarin) (PhDC)

compounds mentioned is available. In previous theoretical studies, we have studied in detail the molecular, electronic and vibrational structures of the free bis(4-hydroxycoumarin) ligands, as well as the vibrational behavior of their lanthanide complexes [16, 23–28].

In this paper we undertake molecular modeling of the lanthanum(III) complex of PhDC, with the aim of investigating its metal-ligand binding mode, and the most probable molecular geometry, as well as the nature and strength of the metal-ligand interactions. To verify the suggested molecular structure, the vibrational spectra of the model complexes were calculated and compared with experimental values. We believe that the results obtained from our theoretical study will contribute to a better understanding of the molecular properties and behavior of lanthanide complexes in relation to their biological activity.

The elemental analysis and mass spectra of the La(III) complex suggested a metal:ligand ratio of 1:1 and an empirical formula of La(PhDC)(OH)(H_2O) [16]. On the basis of experimental IR and ^{13}C NMR data, a coordination through both deprotonated hydroxylic groups and both carbonylic groups was assumed [16]. It is noteworthy, however, that tetradentate coordination of the deprotonated

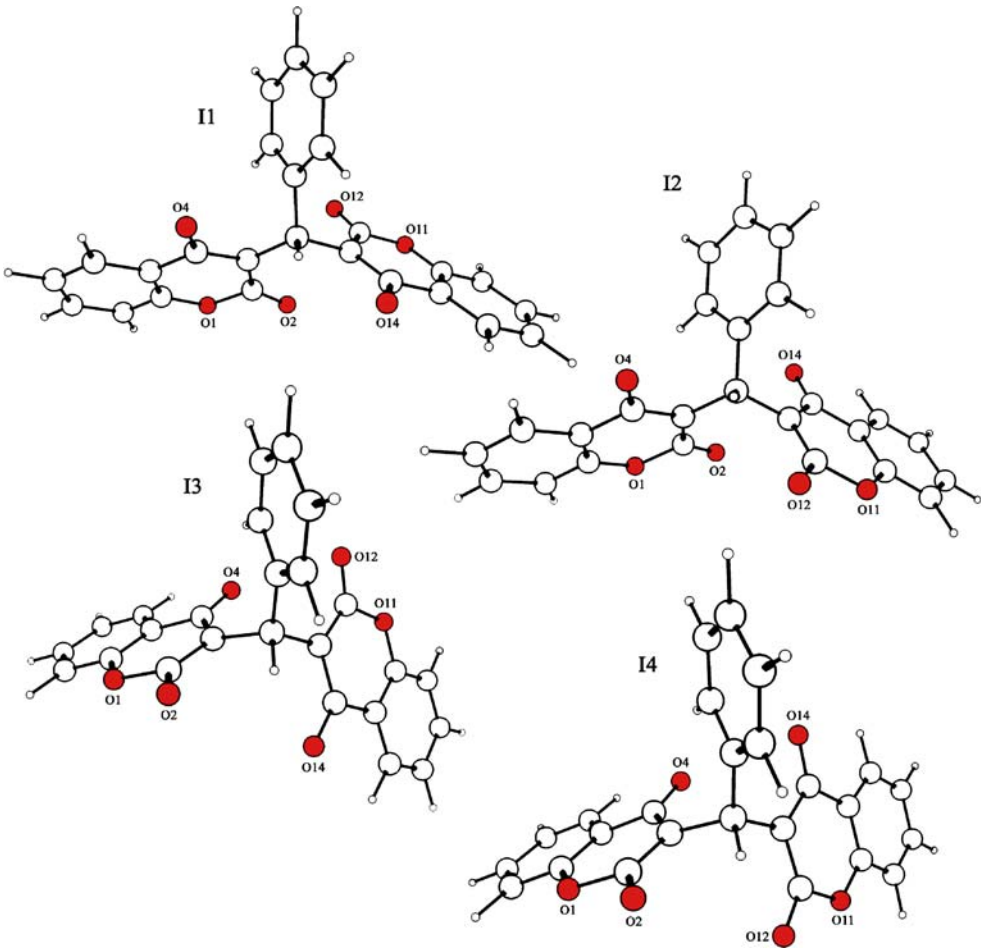

Fig. 2 Low energy deprotonated forms of the ligand ($PhDC^{2-}$) (I1 - I4), optimized with BP86/TZP in a solvent environment

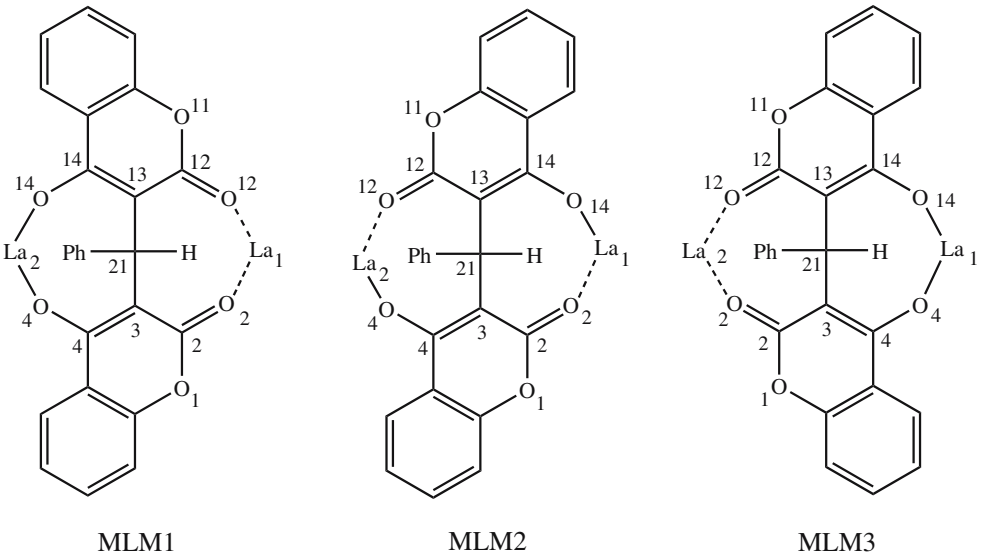

Fig. 3 Schematic presentation of the metal-ligand-metal (MLM) model systems

ligand, $PhDC^{2-}$ (Fig. 2), through both carbonylic (O2, O12) and deprotonated hydroxylic (O4, O14) oxygens to the same lanthanum cation is not feasible. Because of the planarity of the 4-hydroxycoumarin ring, its C=O and C-O^- groups are too distant for coordination to one metal cation. Therefore, in this study, chain structures are modeled assuming that every $PhDC^{2-}$ interacts with two La(III) centers (Fig. 3), and that every La(III) is bound to four oxygen atoms of two different $PhDC^{2-}$ ligands (Fig. 4). In addition, in agreement with the experimental formula La(PhDC)(OH)(H_2O), OH^- and H_2O ligands are included in the model complexes.

Computational methods

All calculations were performed at non-local DFT level of theory using the Amsterdam Density Functional (ADF2005.01) program package, which has been widely utilized for studies of molecules containing heavy elements [29–31]. Density functionals consisting of local density contribution, parameterized by Vosko, Wilk, and Nusair (VWN) [32], and exchange-correlation gradient corrected contribution of Becke [33] and Perdew [34] (BP86) were used. Scalar relativistic effects were considered using the Zero Order Regular Approximation (ZORA) [35–39]. A relativistic valence triple zeta basis set (TZP) with one polarization function was applied for all elements. The $(1s)^2$ core electrons of carbon and oxygen as well as the $(1s2s2p3s3p3d4s4p4d5s5p)^{54}$ core electrons of lanthanum were treated by using the frozen-core approximation. All electron calculations were performed only for PhDC and $PhDC^{2-}$. The numerical integration parameter in ADF was set at 6.0.

Recent investigations have shown that the B3LYP/6-31G (d) level of theory is reliable for the description of the

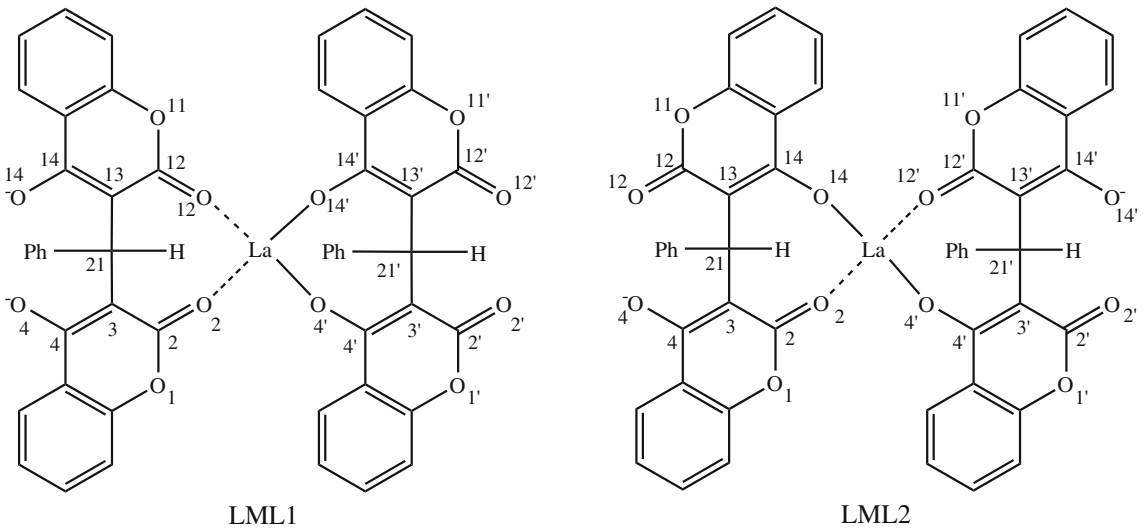

Fig. 4 Schematic presentation of the "tail-head" ligand-metal-ligand (LML) model structures

geometrical, electronic and vibrational structure of bis-coumarins [23–28]. Moreover, the reliability of the B3LYP method in reproducing the ground state geometry of lanthanide complexes has been also demonstrated [40]. Therefore, calculations of PhDC, $PhDC^{2-}$ and model species $[La\text{-}PhDC^{2-}La]^{4+}$were also carried out with the non-local hybrid density functional, B3LYP [41, 42] and 6–31G(d) basis set (using the Gaussian 98 package) [43]. For $[La\text{-}PhDC^{2-}La]^{4+}$ model systems, the core electrons of lanthanum are described with quasi-relativistic effective core potential (ECP) optimized by the Stuttgart-Dresden group, SDD [44, 45, 46]. The ECP replaces 46 core electrons and considers 5s, 5p, 5d and 6s shells in the valence space. The corresponding valence basis set is 7s6p5d contracted to 5s4p3d.

All structures were optimized without symmetry constrains. The minima on the potential energy surfaces are qualified by the absence of negative eigenvalues in the diagonalized Hessian matrix. The vibrational modes are analyzed by means of atom movements, calculated in Cartesian coordinates and by visual inspection of the vibrational modes animated with the ChemCraft program [47]. Frequency calculations of the large model systems $[PhDC^{2-}La\text{-}PhDC^{2-}]^{-}$ and $[La(PhDC^{2-})_2(OH)(H_2O)]^{2-}$ would require significant amounts of computational time and were not performed.

Since the deprotonated form of the ligand, $PhDC^{2-}$, is the active form in aqueous solution, its conformational behavior and molecular properties were investigated in the solvent (water) environment using the COSMO solvation model [48–50] as implemented in the ADF package. Bondi's [51] atomic radii, solvent-accessible-surface and empirical scaling factor of 1.20 were used in the COSMO calculations.

Results and discussion

Molecular geometry of the neutral ligand, PhDC

Our previous studies have shown that the B3LYP/6-31G(d) level of theory is sufficient to reproduce the H-bonded molecular geometry and the vibrational frequencies of PhDC [23]. In this study we used the ADF package, where the B3LYP functional cannot be used for geometry optimizations and therefore another functional has to be selected. The reliability of the BP86/TZP level of theory was checked by comparison with the available X-ray data for PhDC [52].

Selected experimental and calculated (BP86/TZP and B3LYP/6-31G(d) [23]) geometrical parameters are presented in Table 1. Generally, at BP86/TZP level of theory, the C-C bond lengths and C-C-C angles are very close to those calculated with B3LYP/6-31G(d), and are generally a bit larger than the corresponding experimental values. The BP86/TZP C=O bond lengths are longer (1.247, 1.241 Å) with respect to experimental values [1.222(3) Å]. At the same time, the BP86/TZP, O2...O14 and O4...O12 distances obtained were significantly shorter (2.600, 2.565 Å) compared to experimental values (2.720(3), 2.624(3) Å) and B3LYP data (2.696, 2.637 Å). Obviously, the BP86/TZP level of theory produces reliable aromatic C-C bond lengths; however, it overestimates the intramolecular hydrogen bond in PhDC. Therefore, BP86/TZP appears more appropriate for the $PhDC^{2-}$ form where the hydrogen bonds are missing.

Table 1 Selected geometrical parameters (bond lengths in Å, angles in degrees) for the neutral 3,3′-(benzylidene)bis(4-hydroxycoumarin) (PhDC) ligand, calculated at BP86/TZP level of theory and compared to B3LYP/6-31G(d) and experiment

Geometrical parameters[a]	Experimental [52]	B3LYP/6-31G(d) [23]	BP86/TZP
O1-C2	1.366(3)	1.366	1.383
C2-C3	1.445(3)	1.444	1.434
C2=O2	1.222(3)	1.234	1.247
C3-C4	1.365(3)	1.381	1.390
C4-O4	1.333(3)	1.327	1.329
O11-C12	1.368(3)	1.377	1.388
C12-C13	1.436(3)	1.443	1.436
C12=O12	1.221(3)	1.229	1.241
C13-C14	1.365(3)	1.380	1.386
C14-O14	1.339(3)	1.330	1.338
C21-C3	1.513(3)	1.527	1.526
C21-C13	1.521(3)	1.525	1.524
O4...O12	2.624(3)	2.637	2.565
O2...O14	2.720(3)	2.696	2.600
O2-C2-C3	125.1(2)	125.1	125.1
C3-C4-O4	124.0(2)	125.2	124.7
C13-C12-O12	125.7(2)	125.7	125.7
C13-C14-O14	123.8(2)	124.6	124.1

[a] Atom labels are given in Fig. 1

Conformational behavior and molecular properties of the deprotonated ligand, $PhDC^{2-}$

The active form for coordination to La(III) is $PhDC^{2-}$. After deprotonation, ligand flexibility increases and four global minimum conformations with similar electronic energies were found in the gas phase at B3LYP/6-31G(d) level. Further, these conformations were optimized in the solvent environment at BP86/TZP level. Due to increased repulsion between the negatively charged carbonylic and deprotonated hydroxylic oxygens, the system relaxes by means of simultaneous rotations of the coumarin moieties around the C3-C21 and C13-C21 bonds (Fig. 1). The optimized conformations of $PhDC^{2-}$ in solution, I1, I2, I3 and I4, are

Table 2 Amsterdam density functional (ADF) energy (E, kcal mol^{-1}), solvation energy (E^{solv}, kcal mol^{-1}) and relative ADF energy (ΔE, kcal mol^{-1}) of the $PhDC^{2-}$ conformations optimized with BP86/TZP in aqueous solution

Species[a]	E	E^{solv}	ΔE
I1	−7,318.55	−120.33	0.00
I2	−7,317.66	−120.47	0.89
I3	−7,318.25	−121.17	0.30
I4	−7,316.86	−120.91	1.69

[a] See Fig. 2

given in Fig. 2. The lowest energy (i.e., most stable) structure in solution was I1, followed by I3, I2 and I4 (Table 2). However, the relative energies of the structures in solution are very small (0.30–1.69 kcal mol^{-1}) and do not allow conformers to be reliably distinguished. Therefore, all four structures were considered for coordination to La(III).

To estimate the electron density distribution in $PhDC^{2-}$ conformations, several molecular properties were calculated in the solvent environment. Atomic charges derived from Hirshfeld analysis [53, 54] and electrostatic potential values at the nuclei due to the valence electrons and other nuclei are presented in Table 3. In addition, Nalewajski-Mrozek bond orders based on the valence indices obtained from partitioning of Tr(PΔP) [55–58] were calculated (selected data presented in Table 3).

As evident from Table 3, in all $PhDC^{2-}$ conformations the atomic charges and the atomic electrostatic potential values at O2, O4, O12, and O14 are very close. The same holds for the corresponding C-O bond orders. According to the calculations, after deprotonation in solution, the C=O and $C\text{-}O^{-}$ groups equalize their properties and are expected to manifest similar coordination behavior in complexation reactions with La(III). This prediction is in agreement with IR and ^{13}C NMR data, which suggest coordination through both deprotonated hydroxylic groups and both carbonylic groups [16]. Among the three oxygen types, the lactonic oxygen shows the smallest negative atomic charge and the smallest electrostatic potential value, hence coordination through this atom was not considered.

Modeling the metal-ligand binding mode and the geometry around the La(III) center

In accordance with the experimental data, and our suggestion of a chain structure for the complex, two types of model fragments are considered. The first includes two La (III) centres attached to one $PhDC^{2-}$ ($[La\text{-}PhDC^{2-}\text{-}La]^{4+}$), denoted further as MLM (metal-ligand-metal) fragment (Fig. 3). The second fragment includes two $PhDC^{2-}$ and one La(III) ($[PhDC^{2-}\text{-}La\text{-}PhDC^{2-}]^{-}$), hereafter termed LML (ligand-metal-ligand) fragment (Fig. 4).

Model fragments MLM

In order to investigate the metal-ligand binding modes realized in the suggested chain structure of the complex, the MLM type model fragments were constructed in all possible manners of bidentate metal-ligand binding. Conformational searches were performed at both B3LYP/6-31G (d) and BP86/TZP levels of theory. The minima structures were confirmed by means of frequency calculations at B3LYP/6-31G(d) level. Three model fragments, MLM1, MLM2 and MLM3, were found as minima on the PES and are schematically illustrated in Fig. 3. In MLM1 and MLM3 structures, La(III) is bound to same type oxygens, whereas in MLM2 La(III) is bound to different type oxygens. Selected geometrical parameters and the relative energies of the species are summarized in Table 4. Both levels of theory yielded the same order of MLM stability: MLM1> MLM2 > MLM3. In the lowest energy MLM1 fragment, one La(III) is bound to both oxygen atoms (O4, O14) of the deprotonated hydroxylic groups at the phenyl group (Ph) site (hereafter referred to as "head"), whereas another La(III) is bound to both carbonylic oxygens (O2, O12) at the methylene hydrogen atom site (hereafter referred to as "tail") (as illustrated in Fig. 3). The MLM3

Table 3 Selected Hirshfeld atomic charges (a.u.), electrostatic potential values at the nuclei (in brackets, a.u.) and bond order values of the $PhDC^{2-}$ in solvent environment

Atom[a]	I1	I2	I3	I4
O1	−0.14 (22.56)	−0.14 (22.56)	−0.14 (22.56)	−0.14 (22.56)
O2	−0.32 (22.66)	−0.31 (22.66)	−0.34 (22.65)	−0.34 (22.65)
O4	−0.34 (22.67)	−0.35 (22.67)	−0.33 (22.67)	−0.32 (22.67)
O11	−0.13 (22.56)	−0.14 (22.56)	−0.14 (22.56)	−0.14 (22.56)
O12	−0.32 (22.66)	−0.36 (22.66)	−0.31 (22.66)	−0.35 (22.66)
O14	−0.36 (22.67)	−0.32 (22.67)	−0.35 (22.67)	−0.32 (22.67)
Bond				
C2=O2	2.05	2.06	2.04	2.04
C4-O4	2.01	2.01	2.00	2.00
C12=O12	2.05	2.03	2.05	2.04
C14-O14	1.99	2.02	2.00	2.00

[a] Atom labels are given in Fig. 2

Table 4 Selected geometrical parameters (bond lengths in Å, angles in degrees) and relative energies (kcal mol^{-1}) for metal-ligand-metal (MLM) model systems

Geometric parameters[a]	MLM1		MLM2		MLM3	
	B3LYP/6–31G(d)	BP86/TZP	B3LYP/6–31G(d)	BP86/TZP	B3LYP/6–31G(d)	BP86/TZP
O1-C2	1.322	1.330	1.321	1.329	1.323	1.332
C2-C3	1.400	1.400	1.400	1.400	1.419	1.419
C2=O2	1.321	1.333	1.318	1.329	1.289	1.296
C3-C4	1.435	1.436	1.434	1.435	1.415	1.413
C4-O4	1.307	1.317	1.309	1.319	1.339	1.351
O11-C12	1.322	1.330	1.323	1.333	1.323	1.333
C12-C13	1.400	1.400	1.420	1.420	1.419	1.419
C12=O12	1.321	1.333	1.287	1.293	1.289	1.296
C13-C14	1.435	1.436	1.414	1.413	1.415	1.414
C14-O14	1.307	1.317	1.341	1.355	1.339	1.351
C21-C3	1.547	1.543	1.548	1.542	1.546	1.540
C21-C13	1.547	1.543	1.545	1.541	1.546	1.543
O2-La	2.187	2.147	2.188	2.147	2.254	2.226
O12-La	2.187	2.147	2.262	2.234	2.254	2.225
O4-La	2.246	2.218	2.236	2.210	2.178	2.143
O14-La	2.246	2.216	2.174	2.131	2.178	2.132
O-La1-O	83.0	85.4	84.4	87.7	86.2	89.9
O-La2-O	82.7	82.7	81.4	82.1	80.4	82.1
Relative energy	0.00	0.00	0.80	0.74	1.91	1.80

[a] Atom labels are given in Fig. 3

structure reveals higher relative energy than the MLM1 structure, with 1.91 kcal mol^{-1} at B3LYP, and with 1.80 kcal mol^{-1} at BP86 level. Smaller than MLM3 relative energy values are obtained for the MLM2 model (0.80 at B3LYP and 0.74 kcal mol^{-1}, at BP86). The ligand conformation in this case resembles the experimental one of the neutral PhDC [52]. Analysis of the geometrical parameters for the MLM structures shows that the BP86 distances C2=O2, C12=O12, C4-O4 and C14-O14, are longer by 0.006–0.014 Å than the corresponding distances obtained with the B3LYP functional. With respect to the B3LYP optimized structures, shorter La-O bonds and larger O-La-O bond angles are obtained with the BP86 functional.

In line with MLM stability, the B3LYP calculated metal-ligand interaction energies (ZPVE- and BSSE-corrected) and binding energies decrease (absolute values) in the order MLM1> MLM2 > MLM3 (Table 5). The absolute values are quite large due to the presence of two La(III) cations and the high Coulomb attraction of the counterions. For comparison, the interaction energy of La(III) and coumarin-3-carboxylic acid ([La-CCA]$^{2+}$) was previously estimated (at the same level of theory) to be −542.2 kcal mol^{-1} [59], which is more negative than half of the interaction energy calculated for MLM1 (−506.7 kcal mol^{-1}). The energy contributions to the total binding energy of the most stable system, MLM1, were estimated using energy decomposition analysis (EDA) [60], implemented in the ADF program. In agreement with the shorter BP86/TZP La-O bond lengths, the BP86/TZP binding energy is computed as more negative (−1,513.3 kcal mol^{-1}) than that of B3LYP/6-31G(d) (−1,481.72 kcal mol^{-1}). According to EDA, the electrostatic contribution (−1,207.9 kcal mol^{-1}) to the La-PhDC^{2-}La total binding energy is about 1.8 times larger than the orbital contribution (−677.6 kcal mol^{-1}). This finding is in agreement with the assumption of the predominantly electrostatic character of the metal-ligand binding in these lanthanum complexes.

The MLM1 and MLM2 models were then used to construct larger fragments composed of one La(III) and two PhDC^{2-} ligands (LML). In order to reduce the calculations, the highest energy MLM3 fragment was not considered.

Table 5 Metal-ligand binding energy (BE, kcal mol^{-1}) and interaction energy (IE, kcal mol^{-1}) of MLM models calculated at B3LYP/6–31G(d) level of theory

Name definition	MLM1	MLM2	MLM3
BE[a]	−1,481.72	−1,481.00	−1,480.19
ΔBE	0.00	0.72	1.53
IE[b]	−1,013.37	−1,012.59	−1,011.77
ΔIE	0.00	0.78	1.60

[a] The binding energy is calculated using the formula $BE = E_{MLM} - E^{SP}\left([2La]^{6+}\right) - E^{SP}(PhDC^{2-})$, SP - single point

[b] The interaction energy is calculated using the equation $IE = E^{ZPE}(MLM) - BSSE - 2E_{La3+} - E^{ZPE}(I1)$, I1- the lowest energy PhDC^{2-} conformer

Model fragments LML

On the basis of MLM1 metal-ligand binding, a larger LML1 fragment was constructed. In the LML1 structure, the La(III) is bound to the carbonylic O2, O12 atoms (H-atom site: "tail") of one ligand molecule, and to the deprotonated O4', O14' atoms (phenyl site: "head") of another ligand molecule, forming "tail-head" binding (see Fig. 4). In the case of MLM2-type binding, three LML2 structures are theoretically feasible: (1) "tail-head"—by analogy with LML1 (Fig. 4); (2) "head-head" where the La (III) cation is bound to the O12, O4 atoms of the first ligand and the O12', O4' atoms of a second ligand (all coordinated oxygens are at the phenyl site); and (3) "tail-tail" structure, where the La(III) cation is bound to O2, O14, O2'and O14' (all located at the H-atom sites in PhDC). It should be mentioned that the "head-head" and the "tail-tail" bindings are complementary, forming alternating units in the chain complex. To investigate the conformational behavior of the ligands around the La(III) cation, "tail-head" LML1 and LML2 fragments were optimized from three different starting geometries: (1) *cis*—the phenyl substituent of the ligands are situated at the same site of the plane defined by the four coordinated oxygen atoms, (2) *trans*—the phenyl rings are situated at the opposite sites with respect to that plane, and (3) *Td*—the La(III) cation and the donor oxygen atoms form a pseudo-tetrahedral structure. The BP86 optimized geometries are presented in Fig. 5, and their

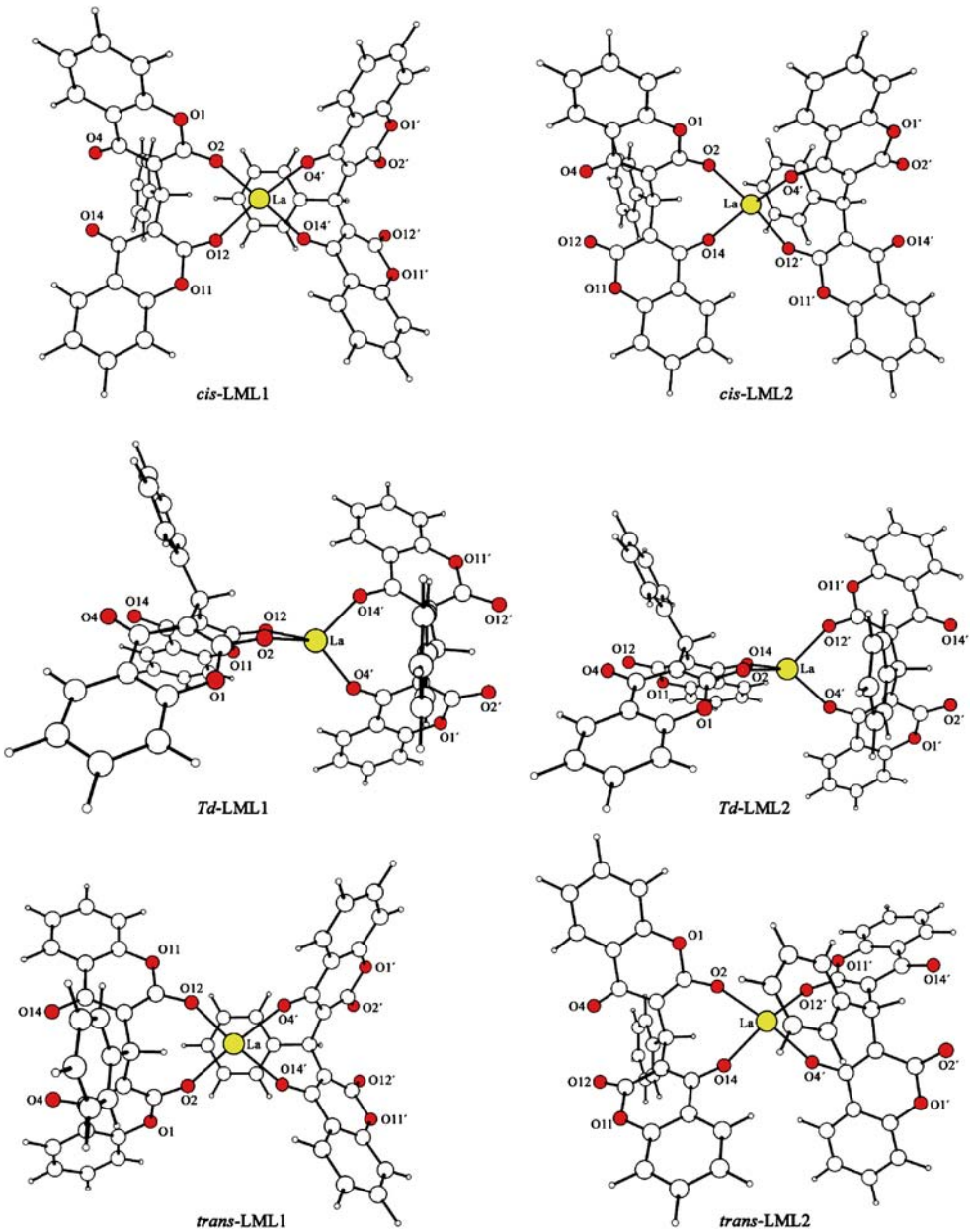

Fig. 5 *cis*-, *trans*- and *Td*-structures based on "tail-head" ligand-metal-ligand (LML1 and LML2) model binding. The structures are optimized at BP86/TZP level of theory

Table 6 ADF and relative energies (both in kcal mol^{-1}) of ligand-metal-ligand (LML) model species calculated at BP86/TZP level of theory

Species[a]	ADF energy	Relative energy
cis-LML1	−14605.87	0.68
Td-LML1	−14603.32	3.23
trans-LML1	−14605.36	1.19
cis-LML2	−14606.55	0.00
Td-LML2	−14602.18	4.37
trans-LML2	−14606.04	0.51

[a] See Fig. 5

ADF energies in Table 6. The relative energies of LML1 and LML2 increase in the order: *cis* < *trans* < *Td*. The lowest energy structure is *cis*-LML2. The *cis*- form of LML1 is 0.68 kcal mol^{-1} higher in energy than *cis*-LML2; however, the differences between the *cis*- and *trans*- forms of LML2 and LML1 are the same: 0.51 kcal mol^{-1}. In spite of the lower MLM1 ADF energy (as compared to MLM2), the LML1 structures are higher in energy than LML2 (with the exception of *Td*-LML1). The energy differences are small and are comparable with the hydrogen bond energies. Hence, the intramolecular interactions involving OH and/or H_2O ligands could reorder the relative stability of the species. Modeling of La-$PhDC^{2-}$ structures including OH and H_2O ligands is therefore essential and is discussed in the next section.

Modeling of $[La(PhDC^{2-})_2(OH)(H_2O)]^{2-}$ fragments

To model the orientations of the $PhDC^{2-}$, OH^- and H_2O ligands around the metal cation, 14 "tail-head" LML1 and LML2 type structures, 2 "head-head" and 4 "tail-tail" LML2 type structures were optimized at the BP86/TZP level of theory.

Three structural groups were considered. In the first, the six oxygen donor atoms form a pseudo-octahedral structure and the OH^- and the H_2O occupy the axial positions of the polyhedron. In the second, the donor atoms occupy the vertexes of a prism-like polyhedron, where the OH^- and H_2O ligands are located at the same side of the plane formed by the donor O-atoms of $PhDC^{2-}$, where they form HO...HOH intramolecular hydrogen bonds. The third group consists of structures based on *Td*-LML1 and *Td*-LML2 model fragments.

The "tail-head" (t-h) structures based on *cis*-, *trans*- and *Td*-LML1 are presented in Fig. 6, and their relative energies are given in Table 7. The calculated energy values showed that the prism-like structures t-hF1 and t-hF4 (t-hF4 < t-hF1) are energetically preferred over the pseudo-octahedral t-hF2, t-hF3, t-hF5 and t-hF6. This trend holds for the "tail-head" structures based on *cis*-, *trans*- and *Td*-LML2 fragments presented in Fig. 7 (energies given in Table 7). The prism-like t-hF8 and t-hF11 reveal lower energies and higher stabilities than the pseudo-octahedral t-hF9, t-hF10, t-hF12 and t-hF13 structures.

"Head-head" and "tail-tail" structures based on *cis*- and *trans*-LML1 model fragments were also calculated and their optimized structures are shown in Fig. 8. With exception of t-tF2, "head-head" binding is energetically preferred over "tail-tail" binding (Table 7). The relative energy values of "head-head" and "tail-tail" structures are comparable with that calculated for "tail-head" fragments.

In summary, among all the optimized structures, the prism-like t-hF1, t-hF4, t-hF8 and t-hF11 fragments and the pseudo-octahedral h-hF1 exhibited the highest stability. The t-hF11 model structure possesses the lowest energy (highest stability) and its stabilization can be explained by the intramolecular hydrogen bond between the proton of the water molecule (H_w) and the hydroxylic oxygen (O_h). Obviously, the prism-like t-hF11 structure based on "tail-head" *cis*-LML2 type binding could be considered as the most probable structure for the La(III) complex of PhDC. The energy differences are small, varying from 1.07 (t-hF4) to 2.52 (t-hF8) kcal mol^{-1}, and hence the higher energy prism-like structure could be also realized. The structures obtained on the basis of tetrahedral LML1 (t-hF7) or LML2 (t-hF14) models showed the lowest stability.

FTIR spectra and vibrational analysis

Comparative analysis of the observed IR spectrum of La(PhDC)(OH)(H_2O) with the calculated vibrational spectra of the model complexes helped understand the La(III)-$PhDC^{2-}$ binding type and hence supported the suggested La(PhDC)(OH)(H_2O) chain structure. Since vibrational calculations for the large model complexes LML and $[La(PhDC^{2-})_2(OH)(H_2O)]^{2-}$ are time- and memory-consuming, a theoretical vibrational study was undertaken only for the MLM1 and MLM2 models, where four ligand oxygen atoms are bound to two La(III) ions. Useful information was derived from the vibrational spectra of PhDC and $PhDC^{2-}$ investigated in our earlier paper [25]. The frequency calculations of the ligand and its La(III) complex make it possibile to discern the ligand modes that are sensitive to the La(III) binding mode, and to investigate their vibrational behavior going from the ligand to its La(III) complex. Full vibrational analyses of MLM1 and MLM2 model complexes were performed, and selected frequencies of the MLM1, MLM2, PhDC and the $PhDC^{2-}$ conformations are given in Table 8. MLM1 was selected as it showed the highest stability. The MLM2 fragment is considered because it was used to construct the most stable LML2

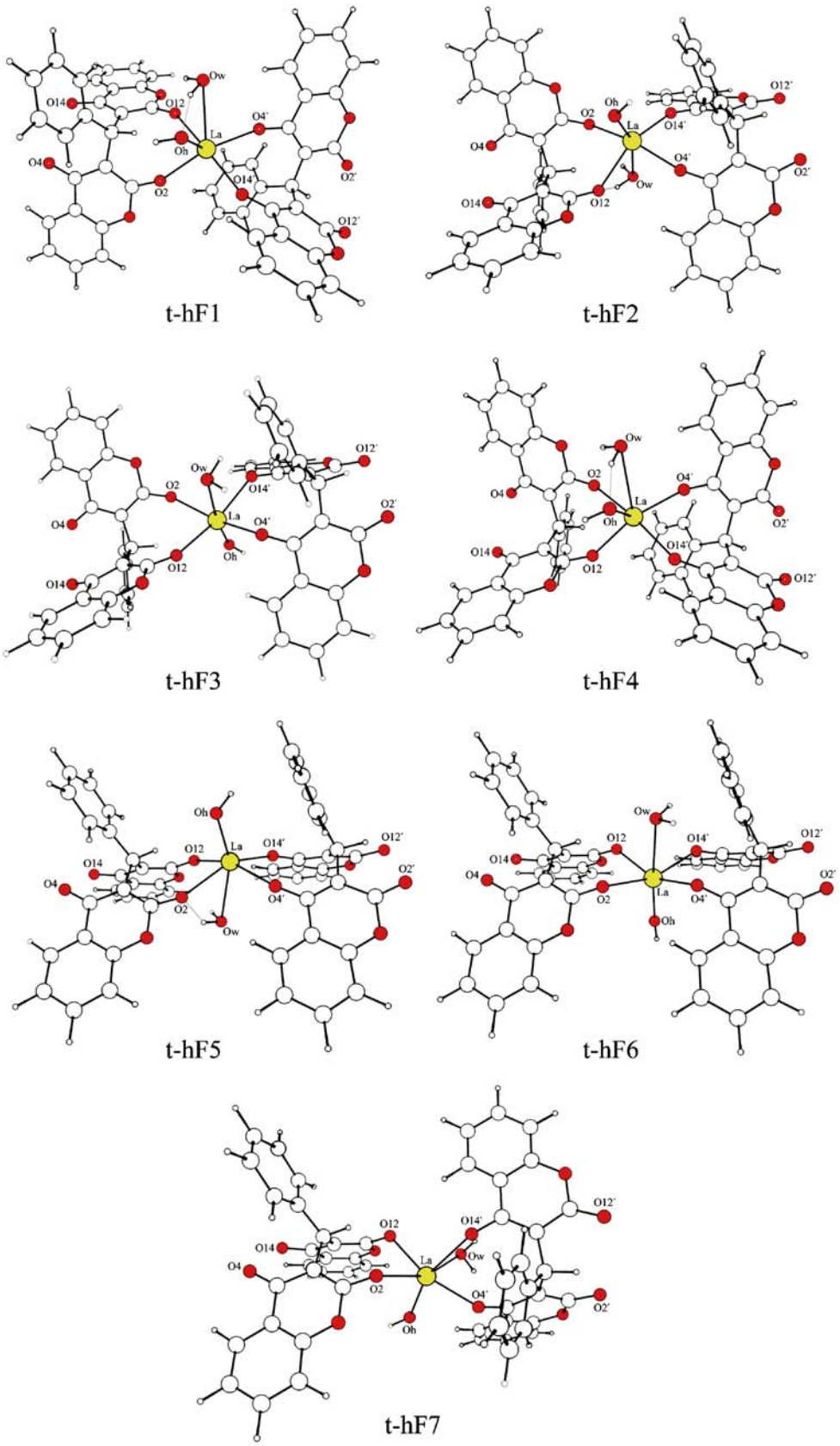

Fig. 6 BP86/TZP optimized $[La(PhDC^{2-})_2(OH)(H_2O)]^{2-}$ model fragments based on *cis* (h-tF4-6), *trans* (h-tF1-3) and *Td* (h-tF7) "tail-head" LML1 model binding

Table 7 ADF and relative energies (both in kcal mol^{-1}) of "tail-head" (t-hF1-14), "head-head" (h-hF1, h-hF2) and "tail-tail" (t-tF1-4) model fragments optimized at BP86/TZP level of theory

Model fragment[a]	ADF energy	Relative energy
"tail-head"		
t-hF1	−15,211.52	2.24
t-hF2	−15,208.66	5.10
t-hF3	−15,207.44	6.32
t-hF4	−15,212.69	1.07
t-hF5	−15,209.08	4.68
t-hF6	−15,208.15	5.61
t-hF7	−15,202.38	11.38
t-hF8	−15,211.24	2.52
t-hF9	−15,209.61	4.15
t-hF10	−15,210.28	3.48
t-hF11	−15,213.76	0.00
t-hF12	−15,210.28	3.48
t-hF13	−15,211.16	2.60
t-hF14	−15,205.77	7.99
"head-head"		
h-hF1	−15,212.35	1.41
h-hF2	−15,208.03	5.73
"tail-tail"		
t-tF1	−15,207.12	6.64
t-tF2	−15,209.85	3.91
t-tF3	−15,206.45	7.31
t-tF4	−15,205.87	7.89

[a] See Figs. 6, 7 and 8

model, as discussed above. The most useful vibrational characteristic for the metal-ligand binding mode in the La (III) complexes is the behavior of the ν(CO) mode. The ν(CO) bands reveal high IR intensity both in the ligand and in the complex spectra and therefore changes in this mode can be tracked with certainty. The remaining stretching modes, containing the La and O4, C4, C3, C2 and O2 atoms, were also given special consideration (Fig. 3). The harmonicity of the calculated frequencies was corrected using the scaling factor 0.965. This factor was derived in our previous study of PhDC [23]. According to the calculations, the most intense band at 1,660 cm^{-1} and the shoulder at 1,646 cm^{-1} in the IR spectrum of PhDC can be assigned to carbonylic ν(CO) vibrations. In $PhDC^{2-}$, the carbonylic bands are shifted to higher frequencies by ~65 cm^{-1}. Obviously, electron organization after deprotonation of PhDC leads to shortening of the carbonylic CO bond lengths. For the MLM1 and MLM2 models, where two La(III) cations are bound to the two carbonylic atoms O2 and O12 (Fig. 3), the calculated carbonylic ν(CO) frequencies are downshifted by 200–260 cm^{-1} as compared to the carbonylic ν(CO) of PhDC, and by 270–324 cm^{-1} as compared to that of $PhDC^{2-}$. Among all the calculated frequencies, the carbonylic ν(C2O2) vibration had the highest IR intensity. The observed IR spectrum of La(PhDC)(OH)(H_2O) revealed that the most intense band is that at 1,508 cm^{-1}. For the MLM2 fragment, which includes one $PhDC^{2-}$ ligand, a lower frequency carbonylic ν(C2O2) vibration was calculated: 1,460 cm^{-1}. For the LML2 model (including two $PhDC^{2-}$ ligands) and for the t-hF11 (including two $PhDC^{2-}$, one OH and one H_2O), we expect the calculated ν(C2O2) vibration to appear at higher frequencies (better fit to experimental data) due to the C2-O2 bond length shortening, MLM2 (1.287 Å) → LML2 (1.280 Å) → t-hF11 (1.266 Å) (Table 9). The medium band at 1,446 cm^{-1} is attributed to the second carbonylic ν(C12O12) vibration. The calculated downshift of ν(C12O12) band, Δ=242 cm^{-1} [1,640 cm^{-1} (PhDC) → 1,398 cm^{-1} (MLM2)] is in good agreement with the observed downshift Δ=194 cm^{-1} (1,640 cm^{-1} → 1,446 cm^{-1}). The predicted smaller downshift of the first ν(C2O2) component (Δ=205 cm^{-1}) compared to that of the second ν(C12O12) (Δ=242 cm^{-1}) correlates well with the observed values, Δ=157 cm^{-1} and Δ=194 cm^{-1}, respectively. The larger downshift of the second ν(C12O12) component explains the splitting of the carbonylic ν(CO) bands at 1,508 and 1,446 cm^{-1}, whereas, in the PhDC, the second ν(CO) component is a shoulder to the main intense carbonylic ν(CO) band. The high intensity bands at 1,619 cm^{-1} and 1,600 cm^{-1} in the IR spectrum of the La (III) complex are attributed to the ν(CC) modes. The same bands are observed in the PhDC spectrum, indicating that they are not affected by La(III) interaction with the ligand.

According to the calculations, the bands observed at 1,345 and 1,336 cm^{-1} in the PhDC spectrum are attributed to the hydroxylic ν(C4O4)/ν(C14O14) vibrations. After deprotonation of PhDC, the hydroxylic ν(CO) bands shift to higher frequencies by ~230 cm^{-1}. In the MLM1 and MLM2 fragments, La(III) ions are connected to the deprotonated hydroxylic oxygens (O4, O14) (Fig. 3) and, as a result, the hydroxylic ν(CO) bands are downshifted by 130–180 cm^{-1} compared to that of $PhDC^{2-}$. Thus, on the basis of the calculations, the observed medium bands at 1,415 and 1,385 cm^{-1} in the IR spectrum of La(PhDC)(OH)(H_2O) are assigned to hydroxylic ν(CO) vibrations. A better fit of the calculated (1,377, 1,344 cm^{-1} for MLM2) to the experimental frequencies is expected for the t-hF11 model, including two $PhDC^{2-}$, one OH and one H_2O, due to the shortening of the calculated C4-O4/C14-O14 bond lengths: from 1.342/1.309 Å for MLM2 to 1.300 Å for t-hF11 (Table 9). The calculated ν(C3C2), ν(C3C4), ν(O1C2) and ν(O1C5) frequencies and their assignments to the observed bands of PhDC and La(PhDC)(OH)(H_2O) spectra are also given in Table 8. Going from PhDC → $PhDC^{2-}$ → MLM2 (MLM1), the frequency changes follow the corresponding bond length changes (Table 9).

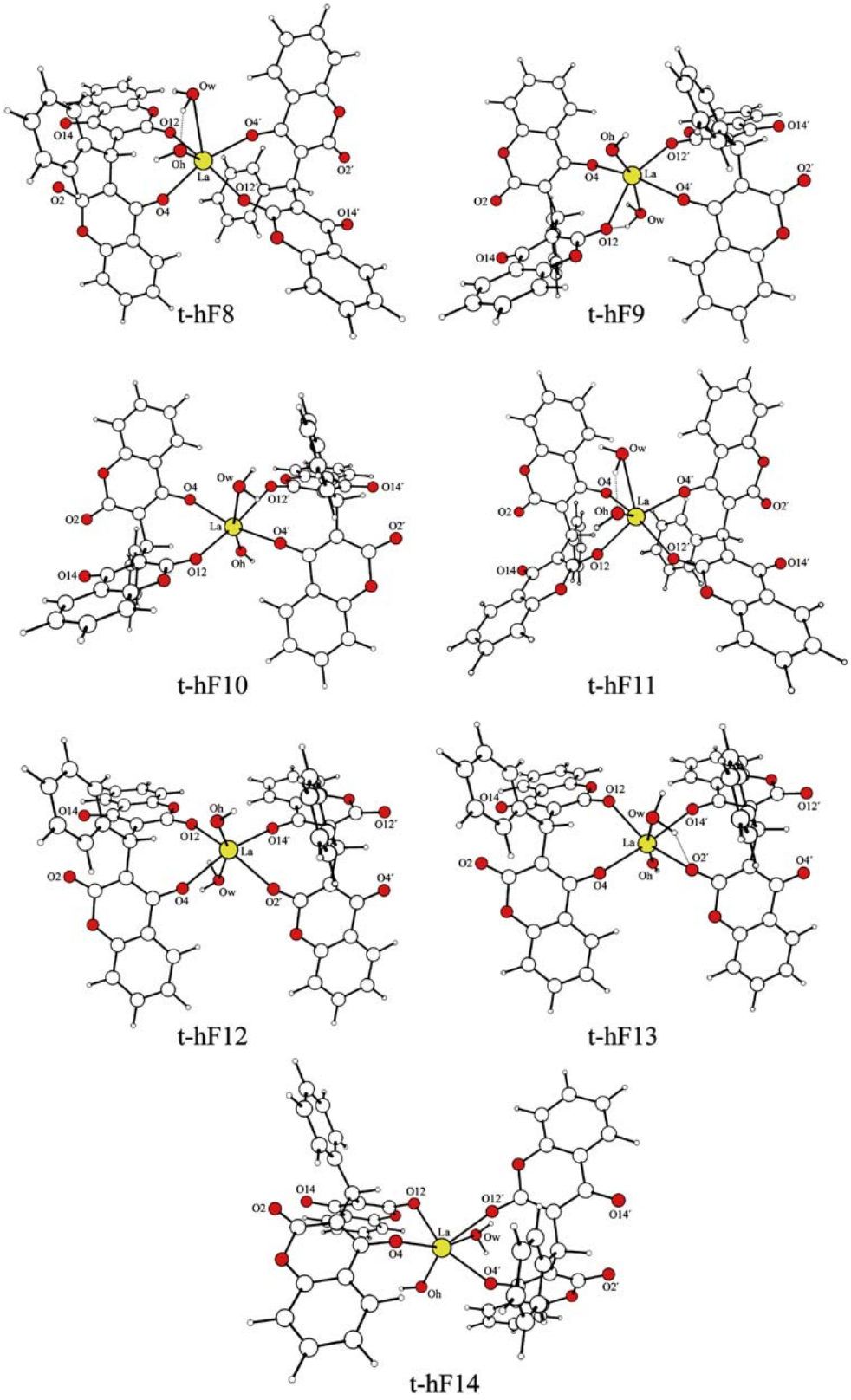

Fig. 7 BP86/TZP optimized $[La(PhDC^{2-})_2(OH)(H_2O)]^{2-}$ model fragments based on *cis* (h-tF11-13), *trans* (h-tF8-10) and *Td* (h-tF14) "tail-head" LML2 model binding

The MLM1 and MLM2 fragments reveal similar vibrational features, and could not be distinguished on this basis (Table 8). The calculated MLM2 spectrum shows better agreement with the experimental IR spectrum of the La(III) complex. The vibrational analysis of the observed IR spectra of PhDC and its La(III) complex, fulfilled on the basis of frequency calculations of PhDC and its model La (III) complexes, confirms the La-PhDC binding type

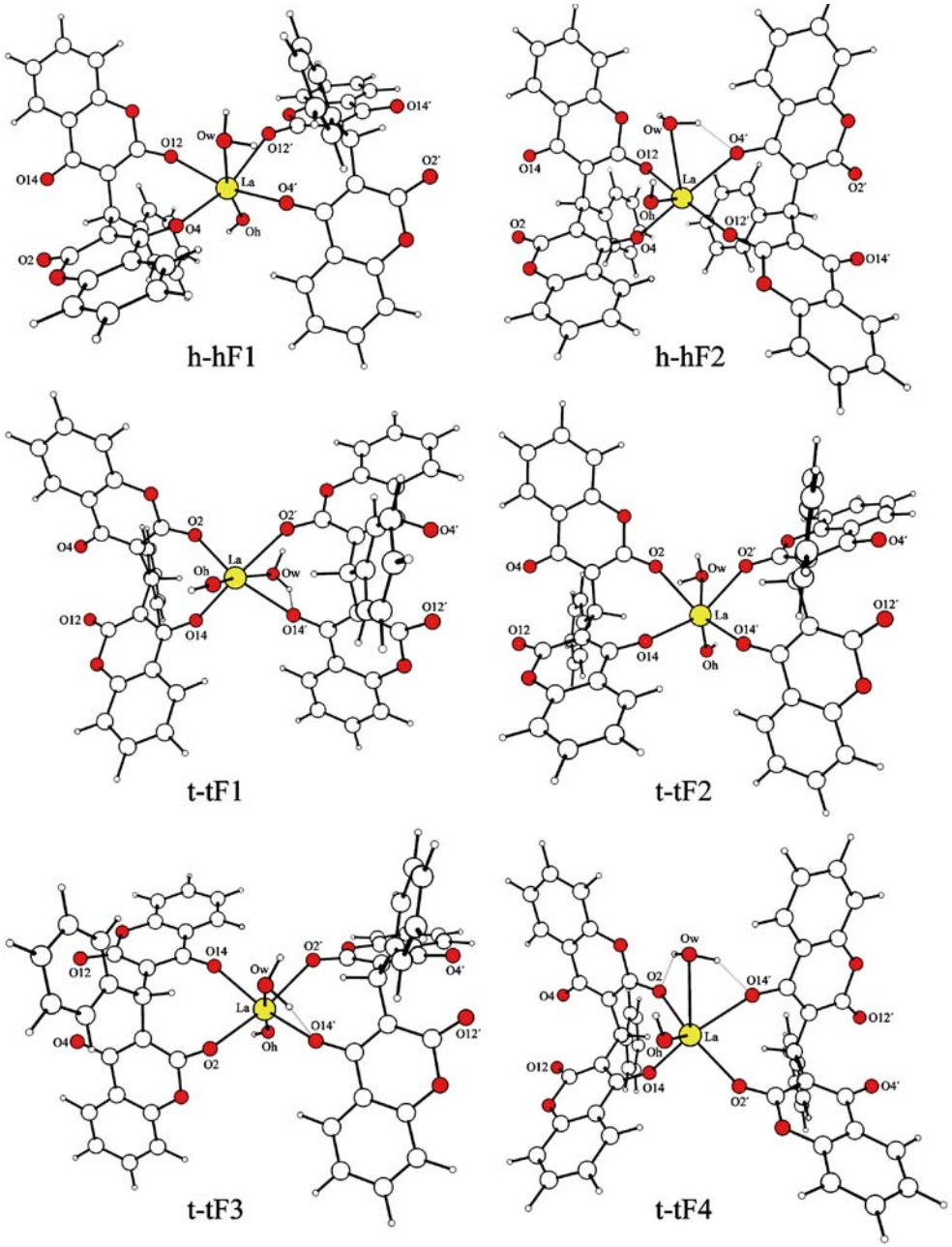

Fig. 8 BP86/TZP optimized $[La(PhDC^{2-})_2(OH)(H_2O)]^{2-}$ model fragments based on "head-head" (h-hF1, h-hF2) and "tail-tail" (t-tF1-4) LML2 model binding

(MLM2) in the suggested chain structure constructed from the t-hF11 fragments.

Summary

The binding mode of 3,3′-(benzylidene)bis(4-hydroxycoumarin) to La(III) and the arrangement of the ligands around the metal cation in the La(PhDC)(OH)(H_2O) complex were investigated using density functional theory methods. The BP86 functional was found reliable for description of PhDC and $PhDC^{2-}$ geometries, although the calculated O...O hydrogen bond distances in the neutral ligand form are a bit shorter. The calculated atomic charges, electrostatic potential values and bond orders of $PhDC^{2-}$ in water solution predicted similar C=O and C-O^- properties and coordination behavior to La(III). Modeling of the two types of fragments (MLM and LML) indicates that La(III)-$PhDC^{2-}$ binding is realized through the chain structure formed by the carbonylic and hydroxylic oxygens. For both LML1 and LML2 type structures, the relative energies increase in the order: *cis* < *trans* < *Td*.

The model calculations of $[La(PhDC^{2-})_2(OH)(H_2O)]^{2-}$ showed that the prism-like structures t-hF11, t-hF8, t-hF4

Table 8 Selected calculated (Calc.) wavenumbers (ν, cm^{-1}) and IR intensities (km mol^{-1}) of PhDC, $PhDC^{2-}$ and La(III)-$PhDC^{2-}$ models compared to experimental (Exp.) values

PhDC			$PhDC^{2-}$	MLM1		MLM2		Compl.	Assign.
Calc.		Exp.	Calc.	Calc.		Calc.		Exp.	
ν	I_{IR}	ν_{IR}	ν	ν	I_{IR}	ν	I_{IR}	ν_{IR}	
1,548			1,667	1,560		1,555			ν(C3C2)
1,480[a]	34	1,496m	1,594[a]	1,491[a]	89	1,487[a]	353	1,559m	
1,544			1,660	1,548		1,554			
1,476[a]	39		1,587[a]	1,491[a]	328	1,486[a]	206		
1,742			1,808	1,491		1,527			ν(C2O2)
1,665[a](as)	1073	1,660vs	1,728[a]	1,425[a](s)	359	1,460[a]	1,111	1,508vs	
1,715			1,785	1,445		1,462			
1,640[a](s)	137	1,640sh	1,706[a]	1,382[a](as)	1193	1,398[a]	617	1,446s	
1,369			1,611	1,472		1,441			ν(C4O4)
1,309[a]	11	1,345m	1,540[a]	1,407[a](s)	349	1,377[a]	511	1,415m	
1,357		1,336m	1,601	1,428		1,411			
1,297[a]	126		1,531[a]	1,366[a](as)	69	1,349[a]	216	1,384m	
1,670			1,421	1,465		1,406			ν(C3C4)
1,597[a]	312	1,617s	1,358[a]	1,401[a]	536	1,344[a]	146	1,362w	
1,655			1,398	1,406		1,400			
1,582[a]	65	1,583w	1,336[a]	1,345[a]	124	1,338[a]	95		
1,254			1,022	1,353		1,350	69		ν(C1O2)
1,199[a]	63		977[a]	1,293[a]	111	1,291[a]		1,254m	
1,241			940	1,330		1,338	38		ν(C1O2)
1,186[a]	64		899[a]	1,271[a]	15	1,279[a]			
1,325			1,287	1,249		1,248			ν(C5O1)
1,267[a]	10		1,230[a]	1,194[a]	62	1,193[a]	70	1,210m	
1,286			1,248	1,243		1,243			ν(C5O1)
1,229[a]	10		1,193[a]	1,189[a]	12	1,189[a]	6		

[a] Scaled frequencies with factor 0.956

and t-hF1 are energetically preferred over the pseudo-octahedral and *Td*-based structures. It was found that, in the prism-like structures, H-bonds formed between a proton of the water molecule (H_w) and a hydroxyl oxygen (O_h) additionally stabilize these structures. The lowest energy prism-like structure, t-hF11, is based on "tail-head" *cis*-LML2 type binding and could be considered as the most probable structure for the La(III) complex of PhDC.

Vibrational analysis of the observed IR spectra of PhDC and its La complex, fulfilled on the basis of frequency

Table 9 Selected bond lengths of the ligand and its La(III) model complexes (in Å)

Bond	PhDC	$PhDC^{2-}$	MLM1	MLM2	*cis*-LML2	t-hF11
C2-O2	1.234	1.220	1.321	1.318	1.295	1.269
C12-O12	1.229	1.217	1.321	1.287	1.280	1.266
C4-O4	1.334	1.260	1.307	1.342	1.325	1.300
C14-O14	1.327	1.256	1.307	1.309	1.308	
C2-C3	1.444	1.423	1.400	1.421	–	–
C12-C13	1.443	1.421	1.400	1.400		
C4-C3	1.381	1.428	1.435	1.434	–	–
C14-C13	1.380	1.421	1.435	1.414		
O1-C2	1.373	1.480	1.322	1.323	–	–
O11-C12	1.377	1.455	1.322	1.321		
O1-C5	1.367	1.346	1.378	1.377	–	–
O11-C15	1.366	1.342	1.377	1.373		

calculations of PhDC and its model La(III) complexes, confirms the La(III)-$PhDC^{2-}$ binding mode (MLM2) in the suggested chain structure (t-hF11 fragment).

Acknowledgments Tzvetan Mihaylov is grateful to Prof. Antonino Zichichi and the World Federation of Scientists for a WFS National Scholarship.

References

1. Suttie JW (1990) Clin Cardiol 13:16–18
2. Bedair AH, El-Hady NA, Abd El-Hatif MS, Fakery AH, El-Agrody AM (2000) Il Farmaco 55:708–714
3. Patonay T, Litkei G, Bognar R, Eredi J, Miszti C (1984) Pharmazie 39:86–91
4. Gnerre C, Catto M, Leonetti F, Weber P, Carrupt PA, Altomare C, Carotti A, Testa B (2000) J Med Chem 43:4747–4758
5. Egan DA, James P, Cooke D, O'Kennedy R (1997) Cancer Lett 118:201–211
6. Masche UP, Rentsch KM, Felten A, Meier PJ, Fattinger KE (1999) Eur J Clin Pharmacol 54:857–864
7. Parrish J, Fitzpatrick T, Tannenbaum L, Patak M (1974) New Eng J Med 291:1207–1211
8. Luzzatto G, Fabris F, Dal Bo Zanon R, Giralami A (1986) Arzneim Forsch 36:972–979
9. Kostova I (2005) Curr Med Chem-Anti-Cancer Agents 5:29–46
10. Kostova I, Manolov I, Karaivanova M (2001) Arch Pharm (Weinheim) 334:157–162
11. Manolov I, Kostova I, Netzeva T, Konstantinov S, Karaivanova M (2000) Arch Pharm (Weinheim) 333:93–98
12. Kostova I, Manolov I, Nicolova I, Konstantinov S, Karaivanova M (2001) Eur J Med Chem 36:339–347
13. Kostova I, Manolov I, Konstantinov S, Karaivanova M (1999) Eur J Med Chem 34:63–68
14. Manolov I, Kostova I, Konstantinov S, Karaivanova M (1999) Eur J Med Chem 34:853–858
15. Kostova I, Manolov I, Nicolova I, Danchev N (2001) Il Farmaco 56:707–713
16. Trendafilova N, Kostova I, Manolov I, Bauer G, Mihaylov T, Georgieva I (2004) Synth React Inorg Metal-Organic Chem 34 (9):1635–1650
17. Kostova I, Kostova R, Momekov G, Trendafilova N, Karaivanova M (2005) J Trace Elem Med Biol 18:219–226
18. Kostova I, Manolov I, Momekov G, Tzanova T, Konstantinov S, Karaivanova M (2005) Eur J Med Chem 40:1246–1254
19. Kostova I, Manolov I, Momekov G (2004) Eur J Med Chem 39:765–775
20. Kostova I, Momekov G (2006) Eur J Med Chem 41(6):717–726
21. Kostova I, Momekov G, Zaharieva M, Karaivanova M (2005) Eur J Med Chem 40:542–551
22. Kostova I, Momekov G, Tzanova T, Karaivanova M (2006) Bioinorg Chem App 2006:1–9
23. Trendafilova N, Bauer G, Mihaylov Tz (2004) Chem Phys 302:95–104
24. Mihaylov Tz, Georgieva I, Bauer G, Kostova I, Manolov I, Trendafilova N (2006) Int J Quant Chem 106:1304–1315
25. Trendafilova N, Kostova I, Rastogi VK, Georgieva I, Bauer G, Kiefer W (2006) J Raman Spectrosc 37:808–815
26. Kostova I, Trendafilova N, Mihaylov Tz (2005) Chem Phys 314:73–84
27. Kostova I, Trendafilova N, Momekov G (2005) JIB 99:477–487
28. Georgieva I, Kostova I, Trendafilova N, Rastogi VK, Bauer G, Kiefer W (2006) J Raman Spectrosc 37:742–754
29. te Velde G, Bickelhaupt FM, van Gisbergen SJA, Guerra CF, Baerends EJ, Snijders JG, Ziegler T (2001) J Comput Chem 22:931–967
30. Guerra CF, Snijders JG, te Velde G, Baerends EJ (1998) Theor Chem Acc 99:391–403
31. ADF2005.01, SCM, Theoretical Chemistry, Vrije Universiteit, Amsterdam, The Netherlands, http://www.scm.com
32. Vosko SH, Wilk L, Nusair M (1980) Can J Phys 58:1200–1211
33. Becke AD (1988) Phys Rev A 38:3098–3100
34. Perdew JP (1986) Phys Rev B 33:8822–8824
35. van Lenthe E, Ehlers AE, Baerends EJ (1999) J Chem Phys 110:8943–8953
36. van Lenthe E, Baerends EJ, Snijders JG (1993) J Chem Phys 99:4597–4610
37. van Lenthe E, Baerends EJ, Snijders JG (1994) J Chem Phys 101:9783–9792
38. van Lenthe E, Snijders JG, Baerends EJ (1996) J Chem Phys 105:6505–6515
39. van Lenthe E, van Leeuwen R, Baerends EJ, Snijders JG (1996) Int J Quant Chem 57:281–293
40. Maron L, Eisenstein O (2000) J Phys Chem A 104:7140–7143
41. Becke AD (1993) J Chem Phys 98:5648–5652
42. Stephens PJ, Devlin FJ, Chabalowski CF, Frisch MJ (1994) J Phys Chem 98:11623–11627
43. Frisch MJ, Trucks GW, Schlegel HB, Scuseria GE, Robb MA, Cheeseman JR, Zakrzewski VG, Montgomery JA, Stratman RE, Burant JC, Dapprich S, Millam JM, Daniels AD, Kudin KN, Strain MC, Farkas O, Tomasi J, Barone V, Cossi M, Cammi R, Mennucci B, Pomelli C, Adamo C, Clifford S, Ochterski J, Petersson GA, Ayala PY, Cui Q, Morokuma K, Malick DK, Rabuck AD, Raghavachari K, Foresman JB, Cioslowski J, Ortiz JV, Baboul AG, Stefanov BB, Liu C, Liashenko A, Piskorz P, Komaromi, I, Gomperts R, Martin RL, Fox DJ, Keith T, Al-Laham MA, Peng CY, Nanayakkara A, Gonzalez C, Challacombe M, Gill PMW, Johnson BG, Chen W, Wong MW, Andres JL, Gonzales C, Head-Gordon M, Replogle ES, Pople JA (1998) Gaussian 98. Gaussian Inc, Pittsburgh PA
44. Dolg M, Stoll H, Savin A, Preuss H (1989) Theor Chim Acta 75:173–194
45. Cao X, Dolg M (2002) J Mol Struct (Theochem) 581:139–147
46. Dolg M, Stoll H, Preuss H (1993) Theor Chim Acta 85:441–450
47. http://www.chemcraftprog.com
48. Klamt A, Schüürmann G (1993) J Chem Soc, Perkin Trans 2:799–805
49. Klamt A (1995) J Phys Chem 99:2224–2235
50. Klamt A, Jones V (1996) J Chem Phys 105:9972–9981
51. Bondi A (1964) J Phys Chem 68:441–451
52. Valente EJ, Eggleston DC (1989) Acta Cryst C45:785–787
53. Hirshfeld FL (1977) Theor Chim Acta 44:129–138
54. Wiberg KB, Rablen PR (1993) J Comp Chem 14:1504–1518
55. Nalewajski RF, Mrozek J (1994) Int J Quant Chem 51:187–200
56. Nalewajski RF, Mrozek J, Michalak A (1997) Int J Quant Chem 61:589–601
57. Nalewajski RF, Mrozek J, Michalak A (1998) Polish J Chem 72:1779–1791
58. Nalewajski RF, Mrozek J, Mazur G (1996) Can J Chem 74:1121–1130
59. Mihaylov Tz, Trendafilova N, Kostova I, Georgieva I, Bauer G (2005) Chem Phys 327:209–219
60. Bickelhaupt FM, Baerends EJ (2000) Rev Comput Chem 15:1–86